High Perform. Polym. **12** (2000) 551–563. Printed in the UK PII: S0954-0083(00)18517-4

X-ray scattering from liquid–liquid interfaces

Mark L Schlossman†, Ming Li, Dragoslav M Mitrinovic and Aleksey M Tikhonov

Department of Physics, University of Illinois, Chicago, IL 60607, USA

E-mail: schloss@uic.edu

Received 31 October 2000

Abstract. We present our recent progress in using synchrotron x-ray surface scattering to study several different aspects of ordering at liquid–liquid interfaces. (1) The interfacial width at the water–alkane interface has been measured for a series of different chain length alkanes. The variation of interfacial width with the carbon number can be described by combining the capillary wave prediction for the width with a contribution from the intrinsic structure. (2) Under appropriate conditions, a surfactant monolayer forms at the interface between water and a hexane solution of a fluorinated surfactant. Reflectivity measurements that probe the electron density profile normal to the interface provide information on the surfactant ordering. This monolayer undergoes a solid to gas transition as a function of temperature. Diffuse scattering near the transition reveals the presence of islands. (3) Equilibrium interfaces between two aqueous phases containing polyethylene glycol and potassium phosphate salts can be studied. We present studies of conformal capillary wave fluctuations between two interfaces of a thin film of this biphase system. We also demonstrate that ferritin can be trapped and studied at this aqueous–aqueous interface.

1. Introduction

An outstanding problem in the area of interfacial phenomena is the determination of the structure at liquid–liquid interfaces. These interfaces play an important role in many chemical and biological systems in addition to being interesting model systems to study the statistical physics of interfaces and membranes. Surfactant molecules naturally arrange themselves at liquid interfaces and, in the case of aqueous–organic interfaces, bring together materials on the microscopic scale that may be otherwise immiscible. Biological membranes which exist at aqueous–aqueous interfaces play a critically important role in many cell processes.

Few experimental techniques are capable of directly probing the molecular order or condensed matter states at a single liquid–liquid interface, nonlinear optical studies being a recently developed, notable exception that provides information on molecular conformations [1–3]. Recently, x-ray and neutron surface scattering have been applied to the study of liquid–liquid interfaces [4–8]. Here, we discuss briefly several investigations that probe fundamental aspects of molecular ordering at liquid–liquid interfaces. In addition, we also discuss a system of potential use for probing biological processes at aqueous–aqueous interfaces.

† Author to whom correspondence should be addressed.

0954-0083/00/040551+13$30.00

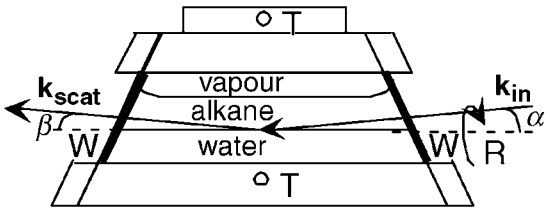

Figure 1. Cross sectional view of a sample cell for water–alkane measurements; W, Mylar windows; T, thermistor to measure temperature; R, rotation about the horizontal used to fine tune the sample flatness. The kinematics of surface x-ray scattering is also indicated: $\boldsymbol{k}_{\rm in}$ is the incoming x-ray wave vector, $\boldsymbol{k}_{\rm scat}$ is the scattered wave vector, α is the angle of incidence and β is the scattering angle.

2. Experiments and discussion

2.1. Experimental methods

These x-ray surface scattering measurements were conducted at beamline X19C at the National Synchrotron Light Source (Brookhaven National Laboratory, USA) with a liquid surface spectrometer and measurement techniques described in detail elsewhere [9]. For x-ray reflectivity, the incident angle α is equal to the scattered angle β (see figure 1). The reflected x-ray intensity is normalized to the incident intensity and measured as a function of the wave vector transfer normal to the plane of the interface, $Q_z = (4\pi/\lambda)\sin(\alpha)$, where $\lambda = 0.0825 \pm 0.0002$ nm is the x-ray wavelength for these measurements. For off-specular diffuse scattering the incident and scattered angles are different.

For measurements at the water–alkane interface, the liquids were contained in vapour-tight, temperature-controlled, polycarbonate or stainless-steel sample cells with Mylar x-ray windows. The x-ray path length through the upper phase is typically 76 mm. The liquids were first stirred and allowed to reach thermal equilibrium. To reduce most of the curvature from the meniscus formed at the cell windows, the windows are angled 25° from the vertical (see figure 1). However, fine tuning of the interfacial flatness is required. This is accomplished by pinning the meniscus to the cell windows (by roughening the windows), and then rotating the entire sample. This twists the interface to yield a very flat region suitable for x-ray scattering.

Measurements at the aqueous–aqueous interface were from liquids placed in a circular teflon trough of diameter 75 mm. This trough was in a temperature-controlled, closed container.

High-purity water was produced from a Barnstead NanoPure system. High-purity alkanes were purchased and then further purified by filtration through basic alumina. The interfacial tension, measured with a Wilhelmy plate, between these purified alkanes and water was constant to within ± 0.1 dynes cm^{-1} as a function of time, where time is measured from the initial formation of the water–alkane interface. Without this purification step, even the highest purity commercially available alkanes showed significant adsorption of impurities to the water–alkane interface as indicated by changes in the interfacial tension of up to 10 to 20 dynes cm^{-1} over a period of a few hours. Other chemicals were used as-received from the manufacturer.

2.2. Water–alkane interfaces

Of fundamental importance in the study of liquid–liquid interfaces is the interface between water and alkanes. This can be used as a model system with which to understand the interactions of alkyl chains with aqueous phases. Here, we show that x-ray reflectivity can be used to measure the interfacial width between water and a series of alkanes.

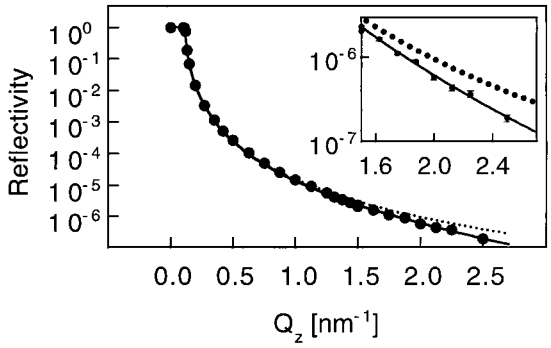

Figure 2. X-ray reflectivity from the water–hexane interface as a function of the wave vector transfer normal to the interface. ●, measurements at 32.00 °C; full curve through the full circles, the fit described in the text; broken curve (squares), the Fresnel reflectivity for an ideal interface. The inset is an expanded view of the high-Q_z region. Error bars on the data are similar to the symbol size in the inset.

X-ray reflectivity measurements as a function of the reflection angle from a bulk interface can be analysed to yield an electron density profile along the normal to the interface (and averaged over the plane of the interface) with a resolution of a fraction of a nanometre [10]. Figure 2 illustrates the x-ray reflectivity, $R(Q_z)$, measured from the water–hexane interface at 32.00 °C [7]. The reflectivity varies with the angle of reflection, α, expressed here in terms of the wave vector transfer normal to the interface, $Q_z = (4\pi/\lambda)\sin\alpha$. Also shown is the Fresnel reflectivity, $R_F(Q_z)$, predicted for an ideal, smooth and flat interface. Both of these curves have a small region of constant reflectivity (equal to one) below a critical wave vector transfer, $Q_c = 0.123$ nm^{-1}, corresponding to a region of total reflection. Both curves then drop off rapidly and smoothly with increasing wave vector transfer.

Although the qualitative features of the ideal and measured curves are similar, the reduction in intensity of the measured reflectivity at larger wave vector transfer is the result of x-rays being scattered by interfacial roughness due to thermally induced capillary wave fluctuations. The classical capillary wave model for the fluctuations [11] corresponds to an error function profile for the electron density averaged over the plane of the interface, $\langle\rho(z)\rangle$. For this interfacial profile the reflected intensity can be expressed as [12]

$$R(Q_z) \cong \left|\frac{Q_z - Q_z^{\mathrm{T}}}{Q_z + Q_z^{T}}\right|^2 \exp(-Q_z Q_z^{\mathrm{T}}\sigma^2) \tag{1}$$

where $Q_z^{\mathrm{T}} \cong \sqrt{Q_z^2 - Q_c^2}$ is the z-component of wave vector transfer with respect to the lower phase. A fit of the data to equation (1) using a single fitting parameter, σ, is illustrated by the full curve in figure 2 and yields the interfacial width $\sigma = 3.5 \pm 0.2$ Å.

In addition to the capillary wave contribution just discussed, the interfacial width may also contain a contribution from an intrinsic profile described, for example, by van der Waals theories [13]. In the spirit of a hybrid model of the interface that describes this intrinsic profile roughened by capillary waves, the total interfacial width, σ_{total}, can be represented as a combination of an intrinsic profile width, σ_0, and the capillary wave contribution [14–16]:

$$\sigma_{\mathrm{total}}^2 = \sigma_0^2 + \frac{k_{\mathrm{B}}T}{2\pi\gamma}\int_{q_{\min}}^{q_{\max}} \frac{q\,\mathrm{d}q}{q^2 + \xi_{\parallel}^{-2}} \equiv \sigma_0^2 + \sigma_{\mathrm{cap}}^2 \tag{2}$$

where k_{B} is Boltzmann's constant, T is the temperature and γ is the interfacial tension, the correlation length, $\xi_{\parallel}$, is given by $\xi_{\parallel}^2 = \gamma/\Delta\rho_m g$ and determines the exponential decay

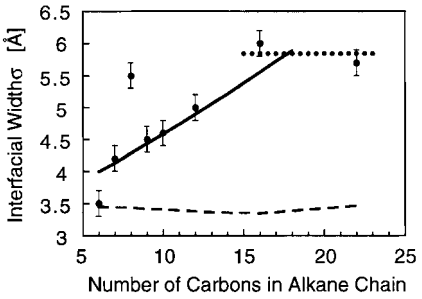

Figure 3. Interfacial width determined by fitting x-ray reflectivity measurements from the water–alkane interface as a function of alkane carbon number. The error bars are determined from statistical and systematic errors. The dashed line indicates the prediction for the interfacial width from capillary wave theory (the rise for C22 is due to a higher temperature). The full line through the lower carbon number data is determined, without adjustable parameters, by combining the capillary wave contribution with an intrinsic interfacial width determined from the gyration radius of the alkane. The horizontal dotted line for the higher carbon numbers is determined, with one adjustable parameter, by combining the capillary wave contribution with an intrinsic width determined from a bulk correlation length described in the text. The three lines indicate calculations for discrete values of the carbon number, but are shown as lines for clarity.

of the interfacial correlations given by the height–height correlation function of interfacial motion [17], $\Delta\rho_m$ is the mass density difference of the two phases, and g is the gravitational acceleration. The wave vector, q, represents the in-plane capillary waves. The limit $q_{\min}$ is determined by the instrumental resolution, which sets the largest in-plane capillary wavelength that the measurement probes. The limit, $q_{\max}$, is determined by the cut-off for the smallest wavelength capillary waves that the interface can support. Direct calculation of σ_{cap} using the literature value of the interfacial tension (51.4 mN m^{-1} at $T = 22\,^{\circ}$C) [18] and $q_{\max} = 2\pi/0.5$ nm^{-1} yields $\sigma_{\text{cap}} = 3.45$ Å, in agreement with our measurement of $\sigma = 3.5 \pm 0.2$ Å. This indicates that the intrinsic profile width, σ_0, is small for this interface.

We have extended these measurements to interfaces between water and longer-chain alkanes [19, 20]. The x-ray reflectivity is similar in form to the measurements in figure 2 and can be fit well with the expression in equation (1). In figure 3 the interfacial width, σ, is plotted against the carbon number. The dashed line indicates the capillary wave prediction for the interfacial width and differs significantly from the values of the width σ fitted to our data. The other two lines in figure 3 are determined by adding, in quadrature, the capillary wave contribution and an intrinsic structural contribution to the interfacial width, σ_0, as in equation (2). For the line that passes through the lower carbon numbers, the intrinsic width, σ_0, is chosen to be the radius of gyration, R_g, of the alkane. Computer simulations have shown that these short alkanes have an R_g expressed as $R_g^2 = C(N)Nl^2$, where l is the carbon–carbon bond length (1.54 Å), N is the number of bonds, and $C(N)$ is a correction factor that varies with bond number [21]. Using the values for R_g from the simulations, the interfacial width is calculated from $\sigma = (R_g^2 + \sigma_{\text{cap}}^2)^{1/2}$, with no adjustable parameters, and is plotted in figure 3. This line shows agreement, within error bars, with the lower carbon number data, except for the water–octane interface. The discrepancy with water–octane is not understood; however, the data are reproducible.

It is expected that the interfacial structure should be independent of chain length for long enough chains. In the case of long chains, it has been shown that adsorption of a polymer melt against a hard wall should be governed by a bulk correlation length [22], $\xi_b \sim \rho_b^{-1/2}$, which we write as $\xi_b = C_b(l\rho_b)^{-1/2}$, where ρ_b is the bulk monomer number density, C_b is an

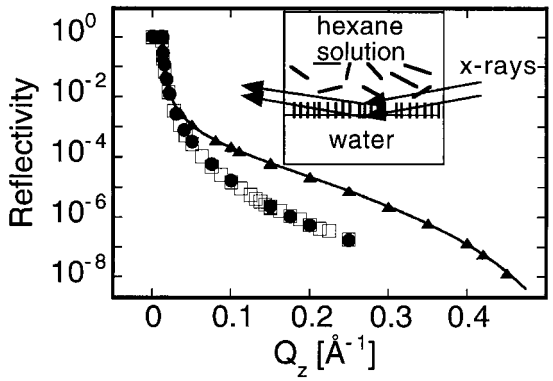

Figure 4. X-ray reflectivity from the water–(hexane solution of $F(CF_2)_{10}(CH_2)_2OH$) interface at $T = 32\,^{\circ}C$, triangles; $T = 48\,^{\circ}C$, full circles; and a pure water–hexane interface at $T = 32\,^{\circ}C$, open squares. The inset is a schematic of the solid surfactant monolayer that forms at $T = 32\,^{\circ}C$.

adjustable parameter of order one, and l is the carbon–carbon bond length. The dotted line for the higher carbon numbers has been adjusted to pass near the values for C16 and C22 by choosing $C_b = 1.09$, which yields $\xi_b = 4.8$ Å. An alternative method to estimate the bulk correlation length is from the x-ray diffraction peaks that correspond to the intermolecular structure in bulk hydrocarbon liquids. The position of the lowest-order peak corresponds to a separation of 4.6 Å, which is close to our estimate for ξ_b [23, 24]. The width from the two longer alkanes we measured possibly indicates a crossover to this long-chain limit.

2.3. Soluble fluorinated surfactants at the water–hexane interface

The few available thermodynamic or spectroscopic measurements indicate that soluble and insoluble amphiphilic monolayers at water–oil interfaces are more loosely packed than the corresponding monolayers at the water–vapour interface [25–27]. In particular, the aliphatic tail groups of the amphiphiles exhibit greater chain disorder, possibly because the oil phase acts as a solvent for the chains at the interface [27]. Therefore, the chains are further from their neighbours than in a close packed solid. This reduces the van der Waals attractive forces between the alkyl chains, but allows for a higher conformational entropy of these flexible chains. Monolayers formed from surfactants soluble in the oil phase are expected to be disordered and in a liquid or gas phase at liquid–liquid interfaces [27].

To explore the ordering in a monolayer of soluble surfactants at the liquid–liquid interface we studied monolayers of $F(CF_2)_{10}(CH_2)_2OH$ (denoted here as $FC_{12}OH$) self-assembled from a solution (2×10^{-3} mol kg^{-1}) in hexane onto the solution–water interface [28, 29]. Figure 4 illustrates the x-ray reflectivity measurements at $T = 32.00(\pm 0.03)\,^{\circ}C$ from the monolayer at the water–(hexane solution) interface [8]. Also shown are measurements from the pure water–hexane interface at the same temperature and measurements from the water–(hexane solution) interface at $T = 48.00\,^{\circ}C$. These curves have a small region of constant reflectivity (nearly equal to one) below a critical wave vector transfer, $Q_c = 0.0123$ Å^{-1}, corresponding to a region of total reflection. The enhanced reflectivity at higher Q_z from the water–(hexane solution) interface at $T = 32.00\,^{\circ}C$ is due to constructive interference of x-rays reflected from the top of the fluorinated monolayer with x-rays reflected from the bottom of the monolayer (inset in figure 4). The reflectivity from the water–(hexane solution) interface at $T = 48.00\,^{\circ}C$ is nearly identical to the measurements from the pure water–hexane interface

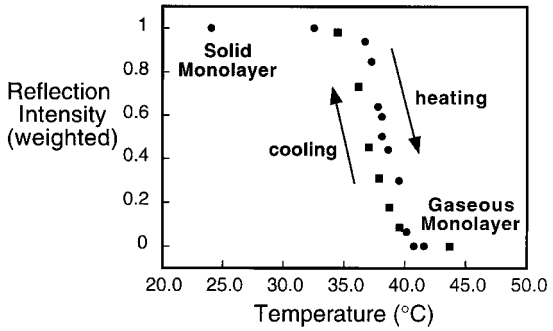

Figure 5. Reflection intensity at $Q_z = 0.1$ Å^{-1} weighted so that a value of one indicates the presence of a solid monolayer phase while the value of zero indicates a gaseous monolayer. This temperature scan reveals hysteresis through the solid–gas monolayer transition of $F(CF_2)_{10}(CH_2)_2OH$ at the water–(hexane solution) interface.

and indicates that most of the $FC_{12}OH$ molecules have desorbed from the interface at this temperature.

These data can be analysed using a general expression, derived from the first Born approximation for x-ray scattering, that relates the reflectivity to the electron density gradient normal to the interface, $d\langle\rho(z)\rangle/dz$ (averaged over the interfacial plane), and written as [10]

$$\frac{R(Q_z)}{R_F(Q_z)} \simeq \left| \frac{1}{\Delta\rho_{bulk}} \int dz \frac{d\langle\rho(z)\rangle}{dz} \exp(iQ_z z) \right|^2 \tag{3}$$

where $\Delta\rho_{e,bulk} = \rho_{e,bulk,lower} - \rho_{e,bulk,upper}$ and $R_F(Q_z)$ is the Fresnel reflectivity predicted for an ideal, smooth and flat interface [30]. The layer of $FC_{12}OH$ is simply modelled as a thin slab of higher electron density sandwiched between two bulk liquids. The interfaces of the top and bottom of this slab are roughened by thermal capillary waves, characterized by the roughness parameter, σ. The reflectivity calculated from (3) using the slab model for the electron density is fitted to the data to yield values for the three fitting parameters: the slab thickness $L = 1.24 \pm 0.03$ nm, $\sigma = 0.36 \pm 0.02$ nm, and the slab electron density $\rho_f = 1.90 \pm 0.04$ (see figure 4) [8].

Our measurement of the electron density of the monolayer at $T = 32.00\,^\circ$C and $\rho_f = 1.90 \pm 0.04$, corresponds to a mass density of 2.19 ± 0.05 g cm^{-3}. This agrees with the density of bulk solid fluoroalkane phases (for example, for n-$C_{20}F_{42}$) which have a density of either 2.23 g cm^{-3} for the monoclinic crystal phase or 2.16 g cm^{-3} for the rhombohedral rotator solid phase [31]. The error bars on our measurement of ρ_f do not allow us to distinguish between these two different solid phases. However, these measurements exclude the possibility that the $FC_{12}OH$ monolayer at the water–hexane interface is in a liquid monolayer phase (bulk liquid fluoroalkanes have a mass density of approximately 1.7 g cm^{-3}) [31, 32].

A similar analysis of the data from the water–(hexane solution) interface at $T = 48.00\,^\circ$C indicates that a conservative upper limit to the surface coverage of $FC_{12}OH$ is approximately 1.5% [8]. The transition from the solid $FC_{12}OH$ monolayer to this gaseous monolayer at higher temperatures can be studied by measuring reflectivity as a function of temperature. Figure 5 indicates the first heating–cooling cycle through this transition.

We believe that the transition region represents an interface with coexisting solid and gas monolayer phases. This is consistent with the enhanced off-specular diffuse scattering that we measured in this transition region. Off-specular diffuse scattering for the heating cycle is illustrated in figure 6. This scattering can be described by the distorted wave Born

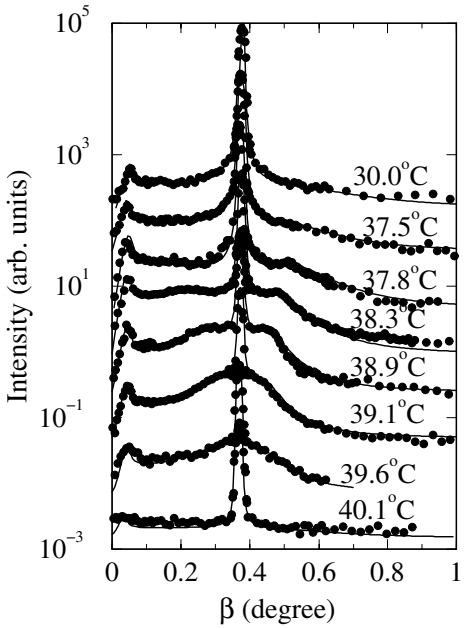

Figure 6. Off-specular diffuse scattering for temperatures scanned through the range of the solid to gas monolayer transition of $F(CF_2)_{10}(CH_2)_2OH$ at the water–(hexane solution) interface. At 30 °C the monolayer is in the low-temperature solid phase; at 40.1 °C it is in the high-temperature gas phase. Additional diffuse scattering in the range 37.5 °C$< T <$ 40.1 °C indicates the presence of islands of the solid phase. The curves are offset for clarity.

approximation as

$$I(\boldsymbol{Q}) \propto |T(\alpha)|^2 |T(\beta)|^2 |F(\boldsymbol{Q})|^2 |S(\boldsymbol{Q})|^2 \tag{4}$$

where α is the incident angle; β is the scattering angle; the wave vector transfer, $\boldsymbol{Q} = \boldsymbol{k}_{\rm scat} - \boldsymbol{k}_{\rm in}$, is the difference between the incoming and scattered wave vectors; $F(\boldsymbol{Q})$ is the form factor for a particle; $S(\boldsymbol{Q})$ is the structure factor for the assembly of particles; and $T(\alpha)$ and $T(\beta)$ are the Fresnel transmission coefficients [33, 34]. The tall, narrow peaks in the centre of the scans in figure 6 occur when the incident angle, α, is equal to the scattering angle, β, and correspond to the specular reflectivity. In figure 6, a small peak appears at small β when $\beta = \theta_{\rm c}$ (the angle for total reflection) and is known as a surface enhancement or Yoneda peak [35, 36].

Here, we are interested in the excess diffuse scattering in the 'shoulders' immediately adjacent to the tall specular peaks in figure 6. The shape of this scattering is determined primarily by the form and structure factors. The shoulders in the measurement at 39.6 °C essentially illustrate the shape of the form factor and reveal the presence of islands (or discs) of the solid phase on the order of a few micrometres in diameter. The sequence of lower temperatures (39.1 °C, 38.9 °C, and 38.3 °C) indicate the presence of additional diffuse scattering due to the assembly of islands. The small peaks that appear in the shoulders of the specular peak indicate that the islands are spatially correlated. As the system is heated from 38.3 °C to 39.6 °C these small peaks move closer to the specular peak. This shows that the islands are spaced progressively further apart as the monolayer undergoes a transition from a solid to a gas phase. Over a narrow range in temperature of less than 0.15 °C (not shown in figure 6) the islands disappear.

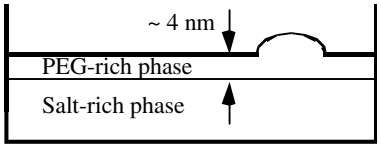

Figure 7. Schematic diagram of a thin film of a PEG-rich phase in equilibrium with a macroscopic PEG-rich reservoir drop (not shown to scale) and a bulk salt-rich phase.

An important feature of the studies into liquid–liquid interfaces is the ability to characterize the role of the upper phase on the structural order within, for example, monolayers at the interface. To gain some insight into the role of the upper-phase hexane on the ordering of the low-temperature $FC_{12}OH$ solid phase monolayers, we studied a similar transition in $FC_{12}OH$ monolayers supported on the water–vapour interface. The $FC_{12}OH$ monolayer was spread in the crystalline island phase at an inverse density of 0.4 nm^2/molecule. Since the crystalline unit cell size is 0.29 nm^2/molecule there is excess area at the interface that allows the monolayer to undergo a transition to a liquid or gaseous disordered phase. X-ray grazing incidence diffraction measurements indicate that an order to disorder phase transition occurs between 58.8 °C and 62.09 °C, slightly more than 20 °C higher than the solid–gas transition in the $FC_{12}OH$ monolayer at the water–(hexane solution) interface. Therefore, the presence of the hexane solvent acts to disorder the monolayer at a lower temperature.

2.4. Aqueous–aqueous interfaces

One of the most tantalizing areas for investigation of liquid–liquid interfaces is biological phenomena. Although biological membranes exist at liquid–liquid interfaces, it has not been previously possible to study molecular ordering and structure on the sub-nanometre scale within a membrane at a liquid–liquid interface. Biological membranes are complex bilayer structures of lipids and proteins. They separate the inside and outside of cells as well as the inside and outside of intracellular organelles within cells. These membranes exist at aqueous–aqueous interfaces and play a critical role in mediating biological communication between cells and the transport of material into and out of a cell.

Although we have successfully applied x-ray reflectivity and diffuse scattering to the study of the liquid–liquid interface, we have not been able to use x-ray grazing incidence diffraction because of the large absorption and background scattering from the upper liquid phase. This diffraction technique allows the in-plane order at an interface to be probed and is likely to be very important in the study of biological structures. Therefore, we chose to develop an aqueous–aqueous interface where the upper phase is a thin film. This was also necessary because of the much larger x-ray absorption that would occur in an upper aqueous phase as compared to the upper alkane phases previously discussed.

Aqueous solutions of polymers and salts are well known to separate into two equilibrium phases. We chose to use biologically compatible polymer and salts: polyethylene glycol (PEG), and potassium phosphates. Once mixed in the proper proportions the resulting solution phase separates into a PEG-rich phase (the lighter, upper phase) and a salt-rich phase. Under the appropriate conditions the PEG-rich phase does not completely wet the salt-rich phase. We extracted the lower, salt-rich phase, and placed a small drop of the PEG-rich phase on its surface. This PEG-rich phase then forms a microscopically thin film (due to partial wetting of the interface) in equilibrium with a reservoir consisting of the remainder of the small drop (see figure 7).

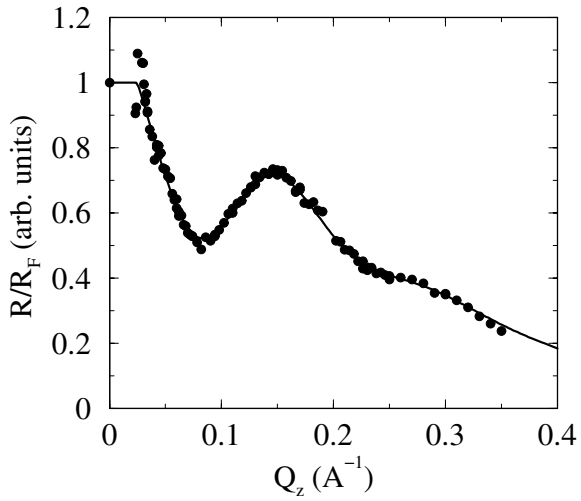

Figure 8. X-ray reflectivity spectra from a thin, partially wet film of a PEG-rich phase on top of a salt-rich subphase. The full curve is a fit described in the text.

Figure 8 shows the x-ray reflectivity (normalized to the Fresnel reflectivity) from this thin film system consisting of PEG (3400 MW):K_2HPO_4:H_2O (13.2:28.9:57.9 wt%) at 35 °C. The oscillations indicate the presence of a thin film of the PEG-rich phase. The full curve in figure 8 is the result of a single slab model analysis of the data using (3). The analysis reveals that the film is 42 Å thick with an interfacial width between the PEG-rich phase and the vapour of $\sigma_{\mathrm{PEG-vapour}} = 3.2$ Å and an interfacial width between the salt-rich and PEG-rich phases of $\sigma_{\mathrm{salt-PEG}} = 8.3$ Å.

A combination of long- and short-range forces is responsible for determining the equilibrium thickness of the thin PEG-rich film. As discussed in the wetting literature, the effect of these forces can be summarized in an interface potential that represents the potential energy between the PEG–vapour and salt–PEG interfaces as a function of the thickness of the film. Both of these interfaces fluctuate with capillary waves. If the fluctuations are conformal (in-phase, see figure 9(a)) then the equilibrium thickness is maintained locally throughout the film. If the fluctuations are non-conformal (or out of phase, see figure 9(b)) then the film thickness varies from point to point throughout the film. From the viewpoint of a local free energy, these variations in thickness will require a free energy penalty. In this local viewpoint we can determine the free energy cost to lowest order by expanding about the minimum of the interface potential. This results in a local modification of the capillary wave Hamiltonian expressed as

$$H = \int \mathrm{d}^2 s \left\{ \sum_{i=1,2} \left[\frac{1}{2} \gamma_i \left(|\nabla \zeta_i|^2 + \left(\frac{\zeta_i}{\xi_{\parallel,cw}} \right)^2 \right) \right] + B(\zeta_1 - \zeta_2)^2 \right\} \tag{5}$$

where i labels the two interfaces, $\zeta_i(x, y)$ represents the local height of each interface above a reference plane whose coordinates are $s = (x, y)$, and B represents the curvature of the interfacial potential near its minimum (we have assumed that the lowest-order term in the interface coupling is quadratic). The Hamiltonian in (5) without the coupling term is the standard capillary wave Hamiltonian for two independent interfaces [11, 17]. This modified Hamiltonian is still Gaussian and can be analysed by standard statistical mechanical methods to yield the ensemble averages of the correlation functions between the amplitudes of the

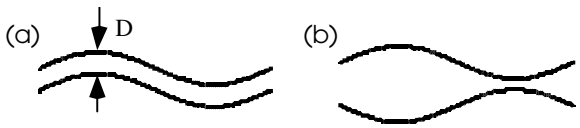

Figure 9. (a) Conformal fluctuations of two interfaces that maintain the local equilibrium film thickness D throughout the entire film. (b) Non-conformal (out of phase) fluctuations in which the film thickness varies throughout the film.

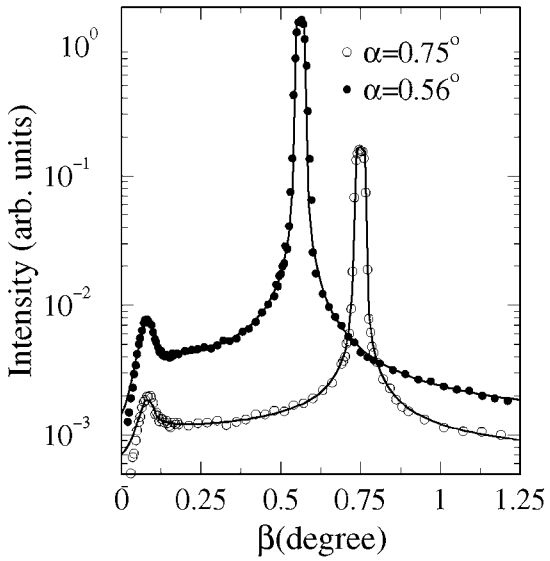

Figure 10. Off-specular nearly transverse diffuse scattering from the capillary wave fluctuations of a thin PEG-rich film on top of a salt-rich subphase. The specular reflectivity for this thin film was shown in figure 8. The lines are fits to a model that contains coupled capillary wave fluctuations between the two interfaces.

capillary waves in reciprocal space. These, in turn, are used to predict the structure factor for off-specular diffuse scattering from the coupled capillary wave fluctuations of the two interfaces.

The interfacial coupling manifests itself experimentally in two ways. In the first, scans in Q_z slightly tuned off the specular condition (nearly longitudinal diffuse scans or so-called background scans) show oscillations that mimic the oscillations in the specular reflectivity curve (not shown). In the second, the form of the off-specular diffuse scattering taken by scanning the exit angle, β, at a fixed incident angle, α, is modified by the interfacial coupling. These latter scans are shown in figure 10. The fits yield a coupling parameter of $B = 7 \times 10^{10}$ J m^{-4}. This indicates an energetic preference for coupling of the interfacial fluctuations as in figure 9(a).

To test the usefulness of this thin-film system for the study of biological macromolecules or membranes, the protein ferritin (from horse spleen, purchased from Aldrich, 100 mg ml^{-1} ferritin in a NaCl 0.15 M solution) was adsorbed to the aqueous–aqueous interface between the thin PEG-rich film and the salt-rich subphase (see figure 11). To reduce the salt concentration to make the solution more favourable to the protein, we used a solution of PEG (8000 MW):K_2HPO_4:KH_2PO_4:H_2O (5:9:6:80 wt%) at 32 °C. Analysis of the x-ray reflectivity

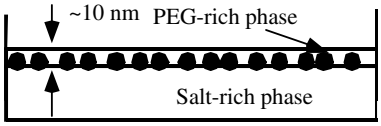

Figure 11. Schematic diagram of the adsorbed protein ferritin (full circles) at an aqueous–aqueous interface.

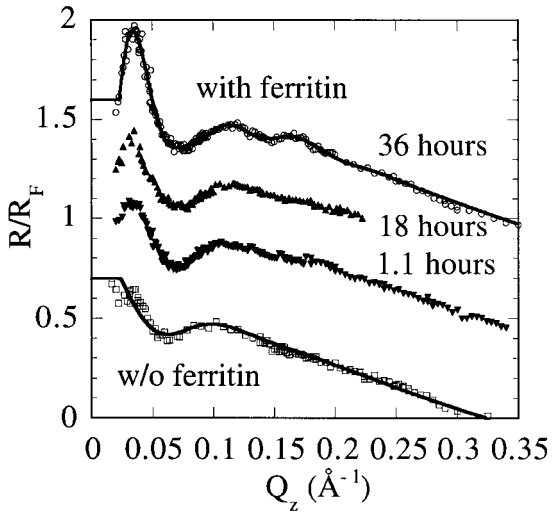

Figure 12. X-ray reflectivity measurements showing the evolution over time of the ferritin layer at the liquid–liquid interface. The lowest curve is the reflectivity before the ferritin is added. The full curve in the upper curve is a fit to a model of ferritin sandwiched between the PEG-rich and salt-rich phases. The curves are offset for clarity.

data from the thin film without the protein (shown in the bottom of figure 12) reveals that the film is 51 Å thick with an interfacial width between the PEG-rich phase and the vapour of $\sigma_{\mathrm{PEG-vapour}} = 3.2$ Å and an interfacial width between the salt-rich and PEG-rich phases of $\sigma_{\mathrm{salt-PEG}} = 15.9$ Å. The protein is added to the interface by injecting 0.8 μl of a ferritin solution into the salt-rich subphase (the solution was prepared by taking 20 μl of the as-purchased ferritin in NaCl and diluting that in 5 ml of a 16 wt% PEG solution). Immediately after adding the protein solution a new peak is present in the reflectivity that indicates an additional electron density at the interface (figure 12). Adsorption of ferritin at the interface continues until, after 36 h, a well developed structure is present in the reflectivity. Our slab model analysis is consistent with the adsorption of ferritin at the liquid–liquid interface.

3. Conclusions

We have used x-ray reflectivity and diffuse scattering to study the molecular ordering at a variety of liquid–liquid interfaces. We have addressed the fundamental issue of ordering at pure water–alkane interfaces and demonstrated significant deviations from the predictions of capillary wave theory. The results indicate the presence of molecular ordering of the alkanes at the interface that can be described in terms of a contribution to the interfacial width due to the intrinsic structure. We have shown that for short alkanes the gyration radius sets the length scale

for the intrinsic structure at the interface with water; for longer alkanes, the intrinsic structure is set by the bulk correlation length. We have also addressed the problem of characterizing the order of an equilibrium surfactant monolayer at the water–hexane interface. X-ray reflectivity was used to determine the thickness and electron density of the monolayer. This revealed that the monolayer is a solid at room temperature and undergoes a transition to a gas phase at higher temperatures. Off-specular diffuse scattering revealed that the solid monolayer breaks up into islands of solid phase in coexistence with the gas phase. As the temperature is increased all the solid islands are converted into a gas phase.

We also demonstrated that microscopically thin films can be formed with equilibrium aqueous biphase solutions. The thickness of the films is on the order of 4–5 nm. Capillary waves on the top and bottom surfaces of these films are correlated. The lower phase of this film is an aqueous–aqueous interface that may prove to be useful for the investigation of biological membranes and macromolecules. In our first study of this nature we investigated the adsorption of the protein ferritin to this interface.

Acknowledgments

We acknowledge David Chaiko (Argonne National Laboratory) for collaborative work on the aqueous–aqueous interface and Zhengqing Huang for assistance with experiments at the Brookhaven National Laboratory. MLS gratefully acknowledges support from the NSF Division of Materials Research, the Petroleum Research Foundation administered by the American Chemical Society, the Chemical Technology Division of Argonne National Laboratory, and the UIC Campus Research Board. The National Synchrotron Light Source at Brookhaven National Laboratory is supported by the Department of Energy.

References

[1] Grubb S G, Kim M W, Rasing T and Shen Y R 1988 *Langmuir* **4** 452
[2] Conboy J C, Daschbach J L and Richmond G L 1994 *Appl. Phys.* A **59** 623
[3] Naujok R R, Higgins D A, Hanken D G and Corn R M 1995 *J. Chem. Soc., Faraday Trans.* **91** 1411
[4] Lee L T, Langevin D and Farnoux B 1991 *Phys. Rev. Lett.* **67** 2678
[5] Phipps J S, Richardson R M, Cosgrove T and Eaglesham A 1993 *Langmuir* **9** 3530
[6] McClain B R, Lee D D, Carvalho B L, Mochrie S G J, Chen S H and Litster J D 1994 *Phys. Rev. Lett.* **72** 246
[7] Mitrinovic D M, Zhang Z, Williams S M, Huang Z and Schlossman M L 1999 *J. Phys. Chem.* **103** 1779
[8] Zhang Z, Mitrinovic D M, Williams S M, Huang Z and Schlossman M L 1999 *J. Chem. Phys.* **110** 7421
[9] Schlossman M L, Synal D, Guan Y, Meron M, Shea-McCarthy G, Huang Z, Acero A, Williams S M, Rice S A and Viccaro P J 1997 *Rev. Sci. Instrum.* **68** 4372
[10] Pershan P S 1990 *Faraday Discuss. Chem. Soc.* **89** 231
[11] Buff F P, Lovett R A and Stillinger F H 1965 *Phys. Rev. Lett.* **15** 621
[12] Nevot L and Croce P 1980 *Rev. Phys. Appl.* **15** 761
[13] Rowlinson J S and Widom B 1982 *Molecular Theory of Capillarity* (Oxford: Clarendon)
[14] Weeks J D 1977 *J. Chem. Phys.* **67** 3106
[15] Braslau A, Deutsch M, Pershan P S, Weiss A H, Als-Nielsen J and Bohr J 1985 *Phys. Rev. Lett.* **54** 114
[16] Schlossman M L 1997 *Encyclopedia of Applied Physics* vol 20, ed G L Trigg (New York: VCH) pp 311–36
[17] Gelfand M P and Fisher M E 1990 *Physica* A **166** 1
[18] Goebel A and Lunkenheimer K 1997 *Langmuir* **13** 369
[19] Mitrinovic D M, Tikhonov A M, Li M, Huang Z and Schlossman M L 2000 *Phys. Rev. Lett.* **85** 582
[20] Tikhonov A M, Mitrinovic D M, Li M, Huang Z and Schlossman M L 2000 *J. Phys. Chem.* **104** 6336
[21] Avitabile G and Tuzi A 1983 *J. Polymer Sci.* **21** 2379
[22] Eisenriegler E 1983 *J. Chem. Phys.* **79** 1052
[23] Habenschuss A and Narten A H 1989 *J. Chem. Phys.* **91** 4299
[24] Habenschuss A and Narten A H 1990 *J. Chem. Phys.* **92** 5692
[25] Yue B Y, Jackson C M, Taylor J A G, Mingins J and Pethica B A 1976 *J. Chem. Soc. Faraday Trans. I* **72** 2685

[26] Messmer M C, Conboy J C and Richmond G L 1995 *J. Am. Chem. Soc.* **117** 8039
[27] Richmond G L 1997 *Anal. Chem.* **69** 536A
[28] Hayami Y, Uemura A, Ikeda N, Aratono M and Motomura K 1995 *J. Coll. Int. Sci.* **172** 142
[29] Takiue T, Yanata A, Ikeda N, Hayami Y, Motomura K and Aratono M 1996 *J. Phys. Chem.* **100** 20 122
[30] Born M and Wolf E 1980 *Principles of Optics* (Oxford: Pergamon)
[31] Schwickert H, Strobl G and Kimmig M 1991 *J. Chem. Phys.* **95** 2800
[32] Starkweather H W 1986 *Macromolecules* **19** 1131
[33] Becker R S, Golovchenko J A and Patel J R 1983 *Phys. Rev. Lett.* **50** 153
[34] Dietrich S and Wagner H 1984 *Z. Phys.* B **56** 207
[35] Yoneda Y 1963 *Phys. Rev.* **131** 2010
[36] Schlossman M L and Pershan P S 1992 *Light Scattering by Liquid Surfaces and Complementary Techniques* ed D Langevin (New York: Dekker) pp 365–403